Carbon Coating Stability on High-Voltage Cathode Materials in H_2O-Free and H_2O-Containing Electrolyte

Michael Metzger,[a,*] Johannes Sicklinger,[a] Dominik Haering,[a,*] Cüneyt Kavakli,[a,] Christoph Stinner,[b] Cyril Marino,[a,**,c,z] and Hubert A. Gasteiger[a,***]**

[a]*Chair of Technical Electrochemistry, Technische Universität München, D-85748 Garching, Germany*
[b]*BMW AG, D-80788 Munich, Germany*

Carbon coatings on cathode materials with low electrical conductivity like phospho-olivines $LiMPO_4$ (M = 3d-transition metal) are known to improve their performance in Li-ion batteries. However, at high potentials and in the presence of water, the stability of carbon coatings on high-voltage materials (e.g., $LiCoPO_4$) may be limited due to the anodic oxidation of carbon. In this work, we describe the synthesis of $LiFePO_4$ (LFP) with an isotopically labeled ^{13}C carbon coating (characterized by Raman spectroscopy, electrical conductivity, and charge/discharge rate capability tests) as a model compound to study the anodic stability of carbon coated cathode materials in ethylene carbonate-based electrolytes. We characterize the degradation of the ^{13}C carbon coating by On-line Electrochemical Mass Spectrometry (OEMS) through the $^{13}CO_2$ and ^{13}CO signals in order to differentiate the anodic oxidation of the coating (^{13}C) from the oxidation of electrolyte, conductive carbon, and binder (all ^{12}C) in the electrode. The oxidation of the carbon coating takes place at potentials $\geq$ 4.75 V for electrolyte without H_2O (< 20 ppm) and $\geq$ 4.5 V for electrolyte with 4000 ppm H_2O, and it is strongly enhanced for H_2O-containing electrolyte. The extent of carbon coating oxidation over 100 h at 4.8 and 5.0 V vs. Li/Li^+ (25°C) is projected on the basis of our OEMS data, suggesting that carbon coatings have insufficient stability at such high cathodic potentials. Furthermore, our results prove the in situ formation of H_2O during the anodic decomposition of ethylene carbonate-containing electrolyte. The H_2O formation is monitored via the detection of gaseous POF_3, which is formed from the reaction of $LiPF_6$ with H_2O.

 [DOI: 10.1149/2.0461507jes]

Manuscript submitted March 3, 2015; revised manuscript received March 26, 2015. Published April 9, 2015. This was Paper 262 presented at the Cancun, Mexico, Meeting of the Society, October 5–9, 2014.

Li-ion batteries are extensively investigated as energy storage devices for electric vehicles (EVs) due to their high energy density and reasonable life time.[1] In order to make EVs competitive with gasoline or diesel cars, and to eventually reduce CO_2 emissions by the electrification of personal mobility, many fundamental challenges still need to be overcome. As summarized by Lu et al.,[2] the battery materials used for today's EVs are graphite and $Li_4Ti_5O_{12}$ (LTO) on the anode and $LiMn_2O_4$ (LMO), $LiNi_xMn_yCo_zO_2$ (NMC), $LiNi_xCo_yAl_zO_2$ (NCA) and $LiFePO_4$ (LFP) on the cathode. In order to increase the driving range of EVs, the energy density (energy per volume) and/or specific energy (energy per mass) of Li-ion batteries needs to be raised. One approach is to employ high-voltage cathode materials that operate at potentials close to 5 V vs. Li/Li^+.[3–5] For example, $LiCoPO_4$ (LCP), a phospho-olivine cathode material, promises a theoretical specific energy of ≈800 mWh/g_{LCP} based on the charge/discharge voltage of ≈4.85 V vs. Li/Li^+ and a theoretical specific capacity of 167 mAh/g_{LCP}.[6]

In contrast to NMC and other layered oxides, phospho-olivines like LFP and LCP suffer from very poor electrical conductivity which limits their rate capability, i.e., their performance at high charge/discharge rates.[7] In the case of LFP, its poor electrical conductivity can be overcome by using small primary particles (0.1–0.5 μm) in combination with an electrically conductive very thin carbon coating (thickness 1–2 nm)[8] applied to the primary particles using different kinds of precursors.[7,9] While uncoated LFP samples either show very poor rate capability or low capacity at rates as low as 0.1 C,[10–12] Lou et al.[13] showed that carbon coated LFP can reach 116 mAh/g_{LFP} at high rates of 10 C (theoretical capacity: 170 mAh/g_{LFP}).[3] Even when the current is increased to 30 C, the discharge capacity can still reach 75 mAh/g_{LFP}, and in the 100th cycle the capacity loss is only 2.3%.[13] Employing acetylene black, sucrose, and glucose as carbon source, Chen et al.[14] presented a carbon coated LFP which is able to reach discharge capacities of 140 mAh/g_{LFP} at 3 C, depending on the respective carbon source. For LCP, however, the preparation and long-term stability of a carbon coating is less straightforward: (i) the deposition of an inert and conductive carbon layer around LCP particles is more complex, since carbo-thermal reduction during synthesis can lead to Co_2P formation;[15] (ii) in its partially and fully delithiated phase, Co^{3+} was shown to react with the carbon coating at high temperature;[16,17] and, (iii) the long-term stability of a carbon coating at the high anodic charge/discharge potentials during LCP cycling is unclear, irrespective of any possible catalytic effect of Co^{3+}.[17] In this context it is also interesting to note that similar cycling stability has been obtained at room temperature for LCP with and without carbon coating.[18]

In the study at hand, we examine the question whether conductive carbon coatings are sufficiently stable against anodic oxidation at potentials relevant for high-voltage cathode materials (≈5 V vs. Li/Li^+). This is accomplished by quantifying the potential-dependent anodic oxidation rate of a carbon coating applied to LFP primary particles. LFP is chosen as a model system for studying carbon coating oxidation, since the preparation of well-characterized homogeneous carbon coatings on phase-pure LCP was not possible due to the above outlined reasons. Thus, the present study focuses on the intrinsic stability of carbon coatings at high anodic potentials without the possibly additional destabilizing effect of Co^{3+}, thus representing a best-case scenario for the anodic stability of the carbon coating. Our study is based on the synthesis of LFP with an isotopically labeled ^{13}C carbon coating obtained from $^{13}C_6$ glucose (i.e., fully ^{13}C isotope exchanged), which allows us to monitor the anodic oxidation of the carbon coating (up to 5.3 V) by quantifying the evolution of the $^{13}CO_2$ and ^{13}CO isotopes using On-line Electrochemical Mass Spectroscopy (OEMS).[19] Since there is ample evidence from the fuel cell literature that the oxidation of carbon can be enhanced by the presence of water,[20,21] the water content of the electrolyte is clearly a critical parameter to describe the degradation behavior of a carbon coating, but also of the conductive carbon, the binder, and the electrolyte. The latter were carefully studied in our recent work,[22] so that we will now focus on studying the anodic stability of a carbon coating using dry electrolyte (< 20 ppm H_2O) and electrolyte with 4000 ppm H_2O in order to

*Electrochemical Society Student Member.
**Electrochemical Society Active Member.
***Electrochemical Society Fellow.
[c]Present address: Paul Scherrer Institut, Electrochemistry Laboratory, CH-5232 Villigen, Switzerland.
[z]E-mail: cyril.marino@psi.ch

simulate the effect of water intrusion over time. $LiClO_4$ is used as a lithium salt in order to avoid the formation of HF with $LiPF_6$,[23] and ethylene carbonate is used as sole solvent in order to minimize the background signals in the mass spectrometric analysis.[22] After a full characterization of the self-synthesized LFP coated with ^{13}C carbon by XRD, Raman spectroscopy, and rate capability tests, the results of the OEMS gas analysis will be presented for the experiments with and without water. Mechanistically, the data suggest that the anodic oxidation of carbon is triggered by the formation of water during the anodic oxidation of ethylene carbonate-based electrolytes at high-voltage, evidenced by OEMS analysis. From these data, we will project the long-term stability of a carbon coating in the potential range corresponding to the charge/discharge voltage of LCP.

Experimental

Synthesis of $LiFePO_4$ (LFP) with isotopically labeled ^{13}C carbon coating.— The syntheses of LFP with and without carbon coating were carried out by applying a hydrothermal method similar to Liang et al.[24] Lithium iron phosphate without carbon coating (further referred to as "LFP_uncoated") was synthesized using a reaction mixture of 75 mmol lithium hydroxide monohydrate ($LiOH \cdot H_2O$, 99.95%, Sigma-Aldrich, Germany), 25 mmol iron(II) sulfate heptahydrate ($FeSO_4 \cdot 7H_2O$, $\geq$ 99.0%, Sigma-Aldrich, Germany) and 27 mmol phosphoric acid (H_3PO_4, 86.3 wt% in H_2O, Sigma-Aldrich, Germany) in 50 ml H_2O (18 MΩcm, Merck Millipore, Germany). The mixture was heated at 180°C for 6 h in a 100 ml Teflon-lined steel autoclave (Berghof BR-100, Germany). For purification, the solid product was centrifuged (Eppendorf Centrifuge 5810 R, Germany) and redispersed in H_2O two times. The obtained solid fraction was dried at 70°C for 5 h under ambient pressure and for 18 h under dynamic vacuum.

^{13}C-coated $LiFePO_4$ (further referred to as "LFP_^{13}C") was synthesized by adding $^{13}C_6$ glucose (D-Glucose, $^{13}C_6H_{12}O_6$, 99 atom% isotopic purity, Cambridge Isotope Laboratories Inc., USA) to the pristine reaction mixture at 15 wt% of the expected LFP mass. The hydrothermal synthesis, product purification, and drying were carried out in the same way as described for LFP_uncoated. Subsequently, an additional annealing step under argon at 750°C for 6 h was applied.

Material characterization.— X-ray diffractograms were recorded in transmission mode with a Stadi P powder diffractometer (STOE & Cie GmbH, Germany) using Cu $K_{\alpha 1}$ radiation ($\lambda = 1.54060$ Å) and a Mythen 1 K detector in the 2θ range 5–50° using step sizes of 0.34° (55 s/step). For each diffractogram four individual ranges were added. Elemental analysis was carried out by CHNS combustion analysis using a Euro EA elemental analyzer (HEKAtech GmbH, Germany). To determine the surface area of the particles, BET analyses were done using an Autosorb iQ nitrogen gas sorption analyzer (Quantachrome Instruments, USA). The conductivity was determined with a self-made tool, measuring the electrical conductivity of powder samples under a pressure of 200 MPa. For this, the sample was filled into a non-conductive tube (6 mm diameter) with a scale bar for measuring the height of the compressed powder, so that the apparent conductivity of the compressed powder could be determined from the compressed powder dimensions and the current flowing at an applied voltage of up to 10 V using a potentiostat (VMP-3, Biologic, France). For Scanning Electron Microscopy (SEM), a JSM-7500F field emission scanning electron microscope (JEOL, Japan) was used at an acceleration voltage of 1 kV and a working distance of 7.2 mm (3300-fold magnification). SEM samples were prepared by transferring the solid powder sample onto a copper tape with adhesive conductive coating (acrylic polymer with copper coated metal backing, 05085C-AB, 3M). Raman spectra were measured with a Senterra Raman spectrometer (Bruker Optics, USA) at a wavelength of 488 nm with a data collection time of 20 s per spectrum.

Electrochemical characterization.— For the electrode preparation, the as-synthesized compound was premixed with carbon black (Super C65, TIMCAL, Switzerland) and polyvinylidene fluoride (PVdF, Kynar HSV 900, Arkema, France) in a mortar at a composition of 80:10:10 (LFP:Super C65:PVdF in wt%) and mixed with N-methyl-2-pyrrolidone (NMP, Sigma-Aldrich, Germany) in a planetary orbital mixer (Thinky, USA) at 2000 rpm and 50 mbar for 15 min. The resulting ink was spread on aluminum foil (thickness 15 µm, MTI Corporation, USA) using a 250 µm gap bar coater (RK PrintCoat Instruments, UK), dried, and subsequently punched into electrodes with 10 mm diameter. These were then pressed (370 MPa, KBr Hydraulic Pellet Press, PerkinElmer, USA) and dried overnight at 120°C under vacuum in a glass oven (drying oven 585, Büchi, Switzerland). The active material loading of the electrodes is 4.0 ± 0.3 mg_{LFP}/cm^2.

The electrochemical measurements were done in Swagelok T-cells, assembled in a glove box with Ar atmosphere (O_2 and $H_2O < 0.1$ ppm, MBraun, Germany), with pure lithium (thickness 0.45 mm, battery grade foil, 99.9%, Rockwood Lithium, USA) as anode, glass fiber separators (glass microfiber filter, 691, VWR, Germany), and 80 µl LP30 electrolyte (1 M $LiPF_6$ in EC:DMC 1:1 wt/wt, < 20 ppm H_2O, BASF, Germany). The cells were cycled with a battery cycler (Series 4000, Maccor, USA) according to the following procedure: 2 cycles at 0.1 C, 2 cycles at 0.2 C and 3 cycles each at 0.5 C, 1 C, 2 C, 5 C and 10 C (referenced to the theoretical capacity of 170 mAh/g_{LFP})[3] between 2.0 V and 4.0 V. A constant voltage (CV) step limited by a current corresponding to C/20 was added at the end of each charge.

On-line Electrochemical Mass Spectrometry (OEMS).— In order to obtain good time resolution in OEMS measurements, it is imperative to use either working-electrodes coated on a porous substrate (e.g., Celgard or glass fiber separator, carbon paper or carbon cloth diffusion media, or metal meshes and foams) or to prepare self-standing working-electrodes; Al or Cu foil-supported electrodes cannot be used, since in this case the diffusional time lag between gas produced in the working-electrode and the battery head space would be too long.[19] In this study, we use self-standing LFP_^{13}C working-electrodes for the following reasons: (i) a high compression is needed to optimize the electrochemical performance of LFP, especially at high C-rates, which would destroy the porosity of the afore-mentioned porous electrode supports; and, (ii) high working-electrode loadings are needed in order to obtain sufficient signal intensity from the anodic oxidation of the isotopically labeled carbon coating which accounts for only 1 wt% of the electrode mass.

The LFP_^{13}C working-electrodes (≈15 mg_{LFP}/cm^2 with 13 mm diameter) were prepared analogously to the way described above, except that the inks were coated onto a glass plate and dried at 60°C for at least 12 h. Subsequently, the coatings were removed from the glass and mixed in a mortar in order to obtain a homogeneous powder, which was pressed into 13 mm diameter pellets under vacuum for 1 h (370 MPa, KBr Hydraulic Pellet Press, PerkinElmer, USA). These electrodes were dried overnight at 120°C under vacuum in a glass oven (drying oven 585, Büchi, Switzerland) and used as working-electrode in our new OEMS two-compartment cell[22] vs. a metallic lithium counter-electrode (diameter 17 mm, thickness 0.45 mm, battery grade foil, 99.9%, Rockwood Lithium, USA). This cell provides a tight seal between the working-electrode (connected to the mass spectrometer via a flow-restricting capillary) and the counter-electrode compartment via a solid Li^+-ion conducting glass ceramic (LICGC, Ohara, Japan) with an additional glass fiber separator (glass microfiber filter, 691, VWR, Germany) on both sides, and thus allows to add water to the working-electrode compartment while maintaining H_2O-free electrolyte in the lithium counter-electrode compartment. In order to avoid HF formation in the cell, ethylene carbonate (EC) with 1.5 M $LiClO_4$ (battery grade for both components, Sigma-Aldrich, Germany) either with or without 4000 ppm H_2O (18 MΩcm, Merck Millipore, Germany) was used as an electrolyte (quantities of water are given per mass of electrolyte throughout the text). Here, 4000 ppm of water are chosen to mimic trace water in the battery cell, as this is an amount which could be easily introduced into the cell if, e.g., the electrodes or the separators had not been dried properly or if the cells had been assembled in ambient air, rather than in a glove box or a dry room. The water

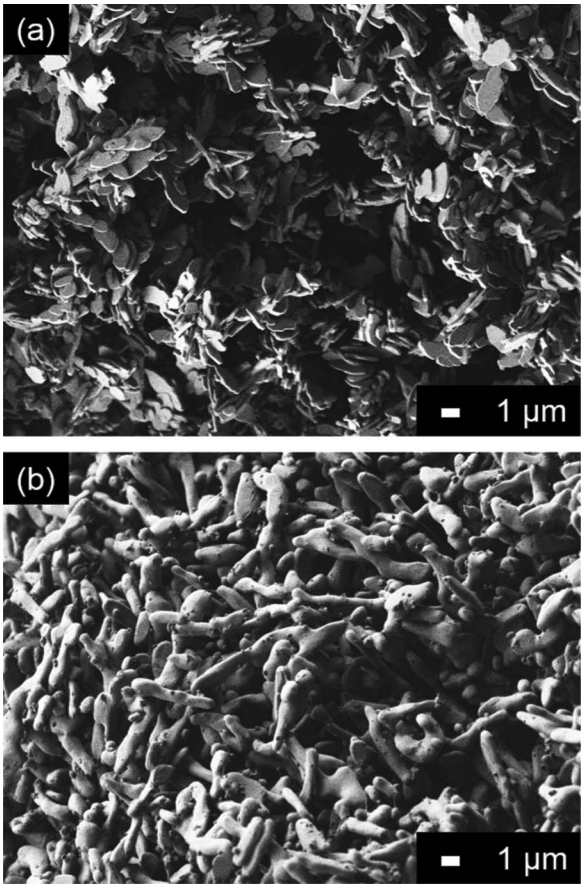

Figure 1. SEM picture of self-synthesized LFP_uncoated (a) and LFP_^{13}C (b).

content of the H_2O-free electrolyte was < 20 ppm, as determined by Karl-Fischer titration (Titroline KF, Schott Instruments, Germany). 160 µl of electrolyte were used in the lower compartment and 500 µl of electrolyte in the upper compartment. Our electrolyte, containing only ethylene carbonate and $LiClO_4$ salt, is clearly not suitable for use in real batteries, but is particularly suitable for mass spectrometry studies, where it produces very low background signals due to its low vapor pressure, which enable highly precise signal quantification as shown in our recent work.[22]

After assembly, the cell was placed into a climate chamber held at 25°C (KB 23, Binder, Germany) and connected to our mass spectrometry system, which has been described elsewhere.[19] To avoid signal fluctuations due to minor pressure/temperature changes, all mass signals were normalized to the ion current of the ^{36}Ar isotope. The cell is first held at OCV for 2 h, followed by a linear sweep voltammetry (LSV) procedure at a scan rate of 0.05 mV/s (Series G300 potentiostat, Gamry, USA) from 3.3 to 5.3 V vs. Li/Li$^+$. The gas evolution during the LSV step is recorded by OEMS. Conversion of the ion currents to concentrations was done for the $^{12}CO_2$ and $^{13}CO_2$ carbon dioxide isotopes, as well as the ^{12}CO and ^{13}CO carbon monoxide isotopes using a calibration gas (Ar with 2000 ppm H_2, O_2, CO and CO_2, Westfalen, Germany) and considering the 1.1% natural abundance of ^{13}C. The ^{12}CO and ^{13}CO amounts were corrected by subtracting 14% of the respective $^{12}CO_2$ or $^{13}CO_2$ signal to account for the mass fractionation of the CO_2 molecule in our setup (for more information on our system specific mass fractionation confer Reference 22).

Results

Characterization of LFP_^{13}C by SEM, XRD, and Raman spectroscopy.— The Scanning Electron Micrographs (Figure 1) reveal very different morphologies for uncoated and carbon coated particles. The LFP_uncoated resembles platelets of ≈0.1 µm thickness and ≈1 µm width. The LFP_^{13}C compound, however, exhibits a rod-like shape with rods of ≈1 µm diameter; the difference in morphology is most likely due to the high-temperature annealing step under argon (750°C for 6 h) which was applied only for the LFP_^{13}C compound. The roughness of the particle surface differs from LFP_uncoated to LFP_^{13}C, suggesting that carbon is indeed covering the surface of the LFP particles in the case of LFP_^{13}C.

Table I. Properties of self-synthesized LFP_uncoated and LFP_^{13}C in comparison to commercial LFP_^{12}C.

Compound	BET [m^2/g]	CHNS [wt%$_C$]	σ [mS/cm]
LFP_uncoated	11	≤ 0.1	< 10^{-7}
LFP_^{13}C	6	1.0	2
LFP_^{12}C (commercial)	17	2.2	30

Table I summarizes the BET surface area, the carbon content determined by CHNS and the electrical conductivity values for LFP_uncoated, LFP_^{13}C, and a commercial carbon coated LFP (LFP_^{12}C by Clariant, Germany) that serves as a reference. As expected, the conductivity values correlate with the carbon content of the samples. The uncoated LFP exhibits an extremely low conductivity (< 10^{-7} mS/cm) compared to the carbon coated samples that have values on the order of several mS/cm. The lower carbon content (1 wt%) of LFP_^{13}C leads to a conductivity of 2 mS/cm compared to 30 mS/cm for LFP_^{12}C with a higher carbon content (2.2 wt%). The surface area of all samples is on the same order of magnitude. The roughly 3-fold lower surface area of LFP_^{13}C compared to LFP_^{12}C can be explained by its lower carbon content (higher carbon contents usually prevent sintering).

Powder X-ray diffractograms (Figure 2a) of LFP_^{13}C (purple line) and LFP_uncoated (green line) are in good agreement with the theoretical XRD pattern (Pnma, a = 10.329 Å, b = 6.006 Å, c = 4.690 Å)[25] of LFP (LFP_theoretical, gray line). Two minor reflections at 2θ = 22.2° and 23.2° reveal the presence of small amounts of a Li_3PO_4 side phase in the LFP_uncoated material. This side phase is also present in commercial LFP_^{12}C (according to the supplier's data sheet).

Raman spectra (Figure 2b) were recorded to characterize the carbon coating around the LFP particles. For LFP_uncoated (green line in Figure 2b), a strong band occurs at 950 cm^{-1}, which is ascribed to the symmetric stretching vibration of the PO_4 unit in the LFP olivine structure.[26] The bands at 998 cm^{-1} and 1068 cm^{-1} correspond to a higher vibration mode[26] and the bands between 200 cm^{-1} and 600 cm^{-1} reveal the presence of minor Fe^{3+} impurities for LFP_uncoated.[27] In case of the carbon coated samples (red line for LFP_^{12}C, purple line for LFP_^{13}C), even the most prominent LFP band at 950 cm^{-1} is extremely weak compared to the strong carbon D- and G-bands around 1350 cm^{-1} and 1600 cm^{-1}. While this strong attenuation of the LFP bands by the carbon coating (thickness ≈1 nm, estimated for a homogeneous coating with a density of ≈2 g/cm^3 using the wt%$_C$ and the BET area given in Table I) is surprising based on the reported penetration depth of the Raman laser radiation through carbon of ≈30 nm,[28] it is nevertheless consistent with most other Raman spectra on carbon coated LFP.[13,29,30] With this in mind, the low intensity of the LFP band at 950 cm^{-1} for the carbon coated samples in Figure 2b indicates a uniform and homogeneous distribution of carbon around the LFP particles, since the laser beam is not focused on a single particle, but has a spot diameter of ≈5 µm, which is ≈5 times larger than the average particle diameter (see Figure 1).

The position of the D-band at 1351 cm^{-1} and the G-band at 1603 cm^{-1} for LFP_^{12}C is in good agreement with the literature D-/G-band values for carbon coated LFP of 1351/1605 cm^{-1} and 1352/1582 cm^{-1} reported in References 13 and 30. Interestingly, an isotope shift can be observed for LFP_^{13}C, with the D- and G-band shifted to 1298 cm^{-1} and 1547 cm^{-1}, respectively. This corresponds to a shift in wavenumbers of ≈3.9%, which is the expected isotope shift of

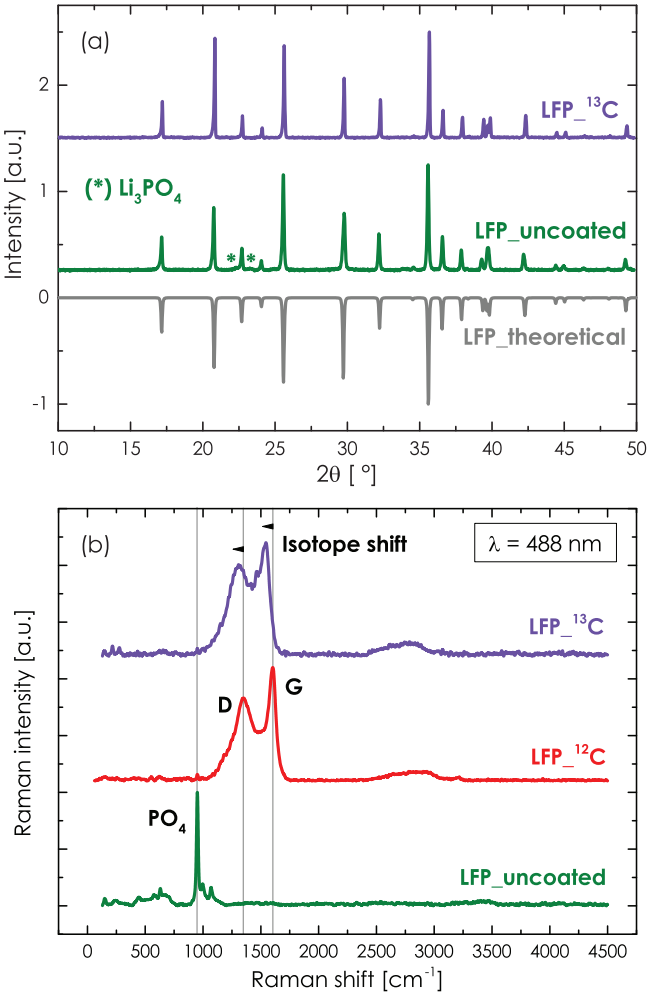

Figure 2. (a) X-ray diffractograms of LFP_uncoated and LFP_^{13}C in comparison to the theoretical diffraction pattern of $LiFePO_4$; (b) Raman spectrum of LFP_uncoated and LFP_^{13}C in comparison to commercial LFP_^{12}C.

$1-\sqrt{12/13}$ resulting from the difference in atomic mass of ^{12}C and ^{13}C. In conclusion, our material characterization by SEM, elemental analysis, powder conductivity measurements, XRD, and Raman spectroscopy proves the successful synthesis of LFP particles with a homogeneous isotopically labeled ^{13}C carbon coating.

Electrochemical performance of LFP_^{13}C.— Figure 3 compares the specific discharge capacities at different C-rates of the self-synthesized LFP_uncoated (green line) and LFP_^{13}C (purple line) with that of the commercial LFP_^{12}C (red line). At 0.1 C, LFP_^{13}C exhibits a capacity of 143 mAh/g_{LFP}, whereas LFP_uncoated reaches only 70 mAh/g_{LFP}. The measured capacities are in agreement with the known performance improvement by applying a carbon coating to LFP particles.[7,14] For the same C-rate, the commercial LFP_^{12}C presents a capacity (153 mAh/g_{LFP}) comparable to that of the self-synthesized LFP_^{13}C, further proving that the carbon coating made with $^{13}C_6$ glucose was successful. The increasing difference between the commercial (LFP_^{12}C) and the self-synthesized carbon coated LFP (LFP_^{13}C) with increasing C-rate can be explained by the ≈2-fold lower carbon content (with a concomitant ≈15-fold lower electrical conductivity) and by the ≈3-fold lower BET area (and accordingly larger particle size) of the latter (see Table I). Nevertheless, for the subsequent experiments on the anodic oxidation rate of the carbon coating, the electrochemical performance of the LFP_^{13}C is sufficient.

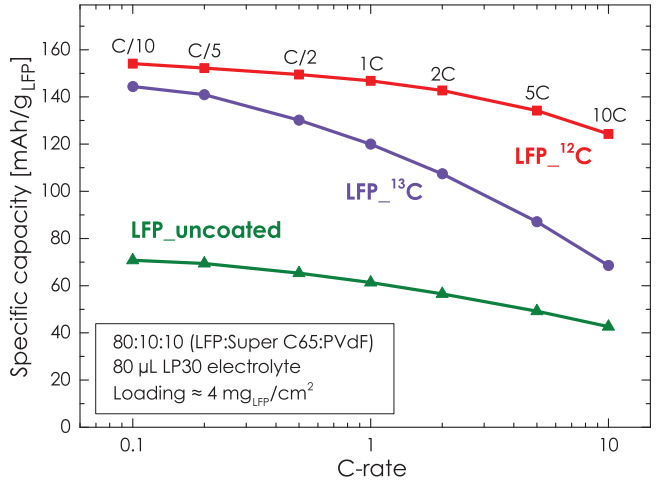

Figure 3. Specific discharge capacity vs. C-rate of LFP_uncoated and LFP_^{13}C in comparison to commercial LFP_^{12}C in LP30 electrolyte performed in Swagelok T-cells.

^{13}C-coating oxidation in H_2O-free electrolyte.— The anodic oxidation rates of the carbon coating of LFP_^{13}C in H_2O-free and H_2O-containing electrolyte are investigated by OEMS using a linear potential scan from 3.3 to 5.3 V at 0.05 mV/s. As the goal of this study is to quantify the anodic oxidation of the ^{13}C-labled carbon coating, we focus on the evolution of carbon monoxide and carbon dioxide, whereby $^{13}CO_2$ (m/z = 45) and ^{13}CO (m/z = 29) can only derive from the labeled carbon coating, as it is the only source of ^{13}C atoms in the system. $^{12}CO_2$ (m/z = 44) and ^{12}CO (m/z = 28), however, can be produced by the anodic oxidation of conductive carbon and PVdF binder in the LFP electrode as well as by the decomposition of the ethylene carbonate-based electrolyte.[21,32,34] In our recent publication,[22] we showed that PVdF is rather stable against anodic oxidation and does not release CO or CO_2, while the anodic oxidation of the conductive carbon (Super C65) and the electrolyte solvent ethylene carbonate (EC) produces significant amounts of CO_2 and CO, resulting in substantial weight loss especially at elevated temperature and in the presence of water. Thus, in the following experiments, the anodic decomposition of conductive carbon and ethylene carbonate is monitored by $^{12}CO/^{12}CO_2$, while the anodic decomposition of the ^{13}C-labeled carbon coating can be tracked exclusively by the formation of $^{13}CO/^{13}CO_2$.

Figure 4 depicts the ion currents, I_Z, normalized by the ^{36}Ar isotope current, I_{36}, of $^{12}CO_2$ (m/z = 44), ^{12}CO (m/z = 28), $^{13}CO_2$ (m/z = 45), and ^{13}CO (m/z = 29) upon a linear sweep voltammetry (LSV) scan from 3.3 to 5.3 V vs. Li/Li^+ in H_2O-free 1.5 M $LiClO_4$ EC electrolyte (< 20 ppm H_2O). The upper panel of the plot (Figure 4a) shows the normalized ion current signals (I_Z/I_{36}) derived from the anodic oxidation of the ^{13}C carbon coating ($^{13}CO_2$ and ^{13}CO, purple lines) as well as from the conductive carbon and the ethylene carbonate ($^{12}CO_2$ and ^{12}CO, magenta lines) after baseline correction. The middle panel (Figure 4b) shows the same data after smoothing, correction for mass fractionation, and conversion into units of [ppm], using a calibration gas (see Experimental Section for details on mass fractionation and calibration). The lower panel (Figure 4c) shows the current-potential curve, mostly reflecting the delithiation of the LFP working-electrode.

In Figures 4a and 4b, $^{12}CO_2$ (dark magenta line), ^{12}CO (light magenta line), $^{13}CO_2$ (dark purple line) and ^{13}CO (light purple line) start to evolve toward the end of the LFP delithiation peak at ≈4.75 V. The $^{13}CO/^{13}CO_2$ signals from the anodic oxidation of the ^{13}C-labeled carbon coating are smaller than the $^{12}CO/^{12}CO_2$ signals from conductive carbon and/or electrolyte oxidation, but they serve as a clear and quantitative proof that the carbon coating on the LFP particles is oxidized at potentials ≥ 4.75 V in dry electrolyte (< 20 ppm H_2O). When reaching 5.3 V at the end of the oxidative scan, the concentrations of $^{12}CO_2$ and $^{13}CO_2$ in the battery head space amount

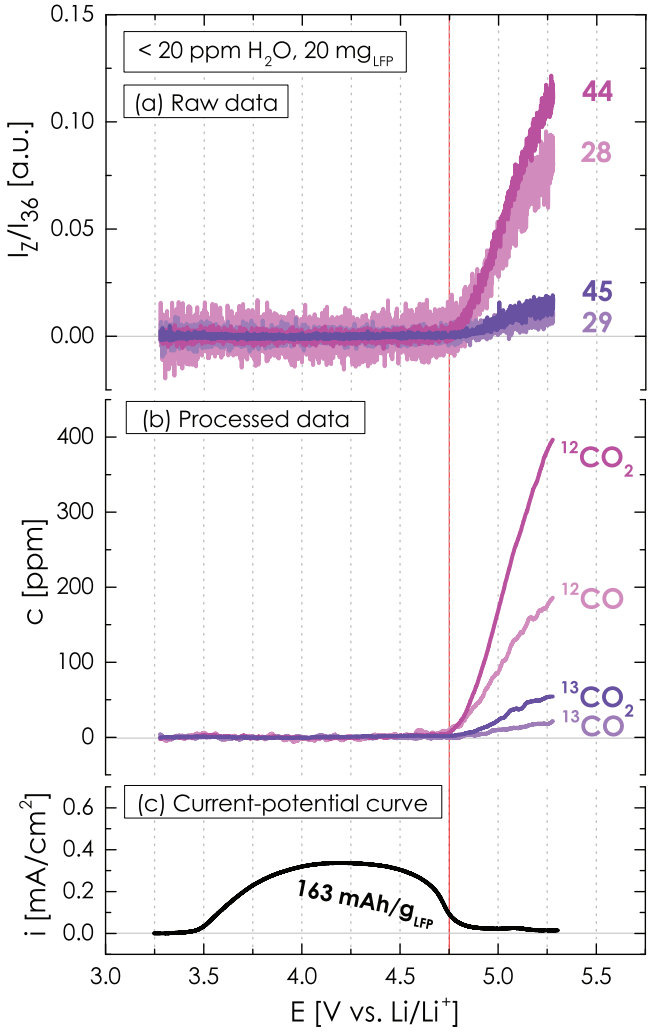

Figure 4. Evolution of CO_2 and CO isotopes as a function of potential for a LFP_^{13}C working-electrode vs. a metallic lithium counter-electrode in a sealed two-compartment cell with 500 µl of 1.5 M $LiClO_4$ in ethylene carbonate (< 20 ppm H_2O) in the working-electrode compartment and 160 µl in the counter-electrode compartment: (a) ion current of the respective isotope I_Z divided by ion current of the ^{36}Ar isotope I_{36} after baseline correction, (b) data after smoothing, correction for mass fractionation, and conversion into units of [ppm], (c) current-potential curve for the linear sweep voltammogram of the LFP_^{13}C working-electrode vs. the metallic lithium counter-electrode from 3.3 to 5.3 V vs. Li/Li$^+$ at 0.05 mV/s.

to 400 ppm and 50 ppm, respectively. The concentrations of the ^{12}CO and ^{13}CO isotopes are roughly 2 to 2.5 times lower, amounting to 190 ppm and 20 ppm, respectively. Table II summarizes the CO and CO_2 concentrations measured at 5.3 V. The extent of the anodic oxidation of the carbon coating and its projected life-time during charge/discharge cycling will be given in the Discussion Section.

Figure 4c shows the potentiodynamic charging profile of the LFP_^{13}C working-electrode. Starting from 3.5 V, a broad LFP_^{13}C delithiation peak is obtained, ending at ≈4.75 V. The thick high-loading electrodes used for the OEMS experiments, in combination with the Li$^+$-ion conductive glass ceramic for separation of the cell compartments, and the model electrolyte comprised of only EC with 1.5 M $LiClO_4$ are likely responsible for the broad LFP signal. The charge capacity of the self-standing LFP_^{13}C working-electrode obtained in the LSV scan (see Figure 4c) amounts to 163 mAh/g_{LFP} and is ≈15% higher than the value obtained under galvanostatic cycling to 4.0 V at 0.1 C (see Figure 3). Compared to the capacity at a galvanostatic charge/discharge at 0.1 C (see Figure 3), the higher specific capacities obtained under these potentiodynamic conditions which also average to a C-rate of ≈0.1 C (9.4 h from 3.3 to 5.0 V) can most likely be rationalized by the overall much higher overpotential applied during charge.

^{13}C-coating oxidation in H_2O-containing electrolyte.— Figure 5 depicts the evolution of $^{12}CO_2$ (m/z = 44), ^{12}CO (m/z = 28), $^{13}CO_2$ (m/z = 45) and ^{13}CO (m/z = 29) upon a linear sweep voltammetry (LSV) scan from 3.3 to 5.3 V vs. Li/Li$^+$ in the 1.5 M $LiClO_4$ EC electrolyte containing 4000 ppm H_2O. According to Yang et al.[33] and our recent article,[22] the addition of water to an EC-containing electrolyte causes a hydrolysis reaction with EC, evidenced by the continuous and potential-independent formation of $^{12}CO_2$ (dark magenta line in Figure 5a). As discussed in our previous work,[22] the H_2O-driven hydrolysis reaction is relatively slow at temperatures < 40°C, but there is also a faster OH^--driven hydrolysis reaction, whereby OH^- is produced at the lithium counter-electrode from water permeating through the polymer edge-seal of the Ohara glass (note that our current two-compartment cell design prevents the mixing of the electrolyte in the two compartments, but still allows for slow permeation of water vapor through the edge-seal, as discussed in detail in Reference 22). Both reactions are potential-independent and start to produce CO_2 already during the OCV period. In Figure 5a (raw data), the OH^--driven hydrolysis of EC can be seen as a continuously increasing $^{12}CO_2$ signal, that is independent of the current-potential profile (Figure 5c), and that was not observed for the dry electrolyte. In the following, any hydrolysis-related contributions to the CO/CO_2 signals are subtracted as background (see gray line in Figure 5a), such that Figure 5b only shows the evolution of CO_2 and CO coming from the anodic oxidation reactions.

For the H_2O-containing electrolyte, the $^{12}CO_2$/^{12}CO and $^{13}CO_2$/^{13}CO signals start to evolve already at a potential of ≈4.5 V (see Figure 5b), which is ≈250 mV lower than without water (compare Figure 4b). Comparing first the total anodic oxidation of the ^{13}C-labeled carbon coating ($^{13}CO_2$ + ^{13}CO) at the positive potential limit of 5.3 V with that of the conductive carbon and ethylene carbonate ($^{12}CO_2$ + ^{12}CO), the enhancement produced by the addition of 4000 ppm H_2O is ≈4-fold in both cases (see Table II). While this suggests a similar water-induced enhancement of the anodic oxidation rates of the carbon coating, the conductive carbon, and the ethylene carbonate, it is interesting to note that the CO_2/CO ratio remains roughly constant for the ^{13}C-labeled carbon coating (≈2.5/1), while it increases in the presence of 4000 ppm H_2O from ≈2/1 to ≈6/1 for the ^{12}C compounds (conductive carbon and ethylene carbonate). The likely reason for this observation will be given in the Discussion Section.

Table II. Concentration of CO_2 and CO derived from the anodic oxidation of conductive carbon/electrolyte ($^{12}CO_2$, ^{12}CO) and carbon coating ($^{13}CO_2$, ^{13}CO) after the LSV scan to 5.3 V vs. Li/Li$^+$ using dry and 4000 ppm H_2O-containing electrolyte based on 1.5 M $LiClO_4$ in EC (data from Figures 4b and 5b).

	From carbon/electrolyte oxidation			From carbon coating oxidation		
H_2O content	$^{12}CO_2$ [ppm]	^{12}CO [ppm]	^{12}CO + $^{12}CO_2$ [ppm]	$^{13}CO_2$ [ppm]	^{13}CO [ppm]	^{13}CO + $^{13}CO_2$ [ppm]
< 20 ppm H_2O	400	190	590	50	20	70
4000 ppm H_2O	2130	350	2480	210	80	290

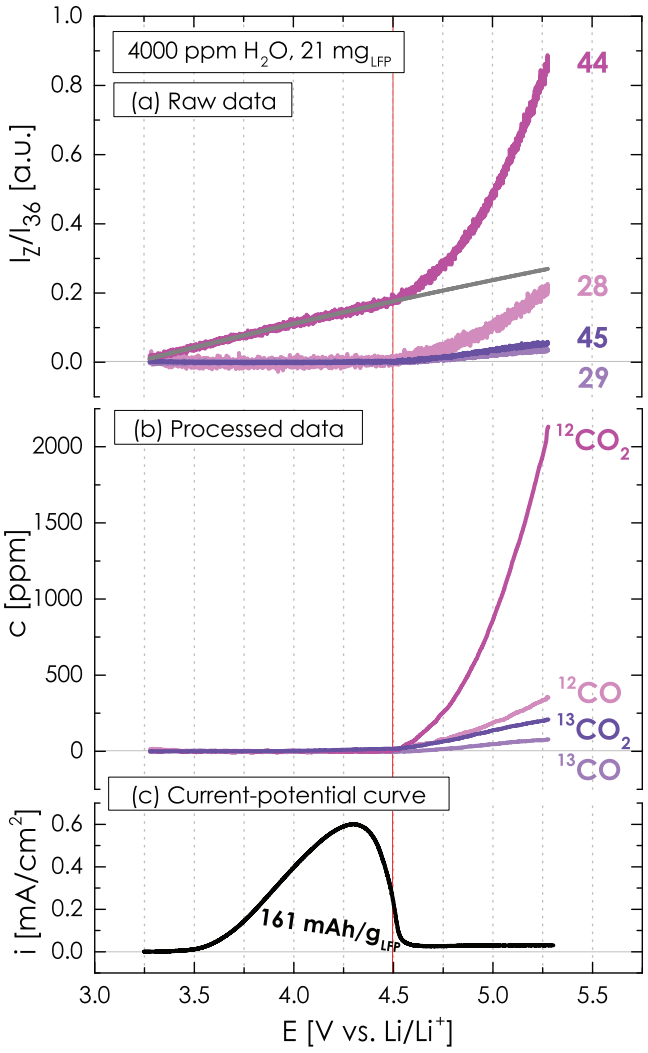

Figure 5. Evolution of CO_2 and CO isotopes as a function of potential for a LFP_^{13}C working-electrode vs. a metallic lithium counter-electrode in a sealed two-compartment cell with 500 µl of 1.5 M $LiClO_4$ EC electrolyte containing 4000 ppm H_2O in the working-electrode compartment and 160 µl dry electrolyte in the counter-electrode compartment: (a) ion current of the respective isotope I_Z divided by ion current of the ^{36}Ar isotope I_{36} with EC-hydrolysis based contribution in gray, (b) data after smoothing, subtraction of the EC-hydrolysis contribution, correction for mass fractionation, and conversion into units of [ppm], (c) current-potential curve for the linear sweep voltammogram of the LFP_^{13}C working-electrode vs. the metallic lithium counter-electrode from 3.3 to 5.3 V vs. Li/Li^+ at 0.05 mV/s.

The very broad LFP delithiation trace observed in dry electrolyte (see Figure 4c) is somewhat sharper in the H_2O-containing electrolyte (see Figure 5c), with the LFP delithiation process completed at a potential of ≈4.5 V. The origin of this phenomenon is not clear at this point.

Discussion

Ethylene carbonate anodic decomposition mechanism.— Based on mostly FTIR and NMR experiments as well as mass spectrometry, Moshkovich et al.[31] proposed a large number of parallel pathways for the electrochemical decomposition of EC at high potential, leading to CO_2 and CO gas formation. At the same time, Zhang et al.[34] presented ab-initio calculations, which proposed a thermodynamically favorable pathway for CO_2 evolution upon the anodic oxidation of EC. In a later, more detailed ab-initio computational study, Xing et al.[32] evaluated several feasible pathways for CO_2 and CO evolution during EC electrooxidation. Both computational studies show the same energetically most favorable initial scission of the EC molecule after electron subtraction (oxidation), resulting in the ring-opened intermediate depicted in Scheme 1. From this point on, two different reaction pathways leading to CO_2 release (as observed by OEMS; see Figures 4 and 5) are thought to be prevalent: (i) path 1 (see Scheme 1), which according to Xing et al.[32] is energetically most favorable, results in the formation of a $^{\bullet}O\text{-}CH_2\text{-}CH_2^+$ leaving group upon CO_2 formation; (ii) path 2, where according to Zhang et al.[34] CO_2 removal occurs simultaneously with an H-transfer, leading to $^{+\bullet}O{=}CH\text{-}CH_3$ as the most likely leaving group. While Zhang et al.[34] do not report on a pathway leading to CO formation, Xing et al.[32] propose another, compared to CO_2 formation (i.e., path 1) energetically less favorable pathway, which can lead to CO release via the formation of formaldehyde and $^{+\bullet}O{=}CH_2$ (see path 3 in Scheme 1).[32] Unfortunately, since the $^{12}CO_2/^{12}CO$ ratio in our experiments is determined by the anodic oxidation of both EC and conductive carbon (Super C65), the data in Table II and in Figure 4 does not allow to quantify the CO_2/CO ratio exclusively due to the anodic oxidation of EC. However, in our previous study using ^{13}C-labeled EC, the CO_2/CO ratio observed upon the anodic oxidation of EC with < 20 ppm H_2O at 25°C is ≈6/1,[22] consistent with the above conclusions by Zhang et al.[34]

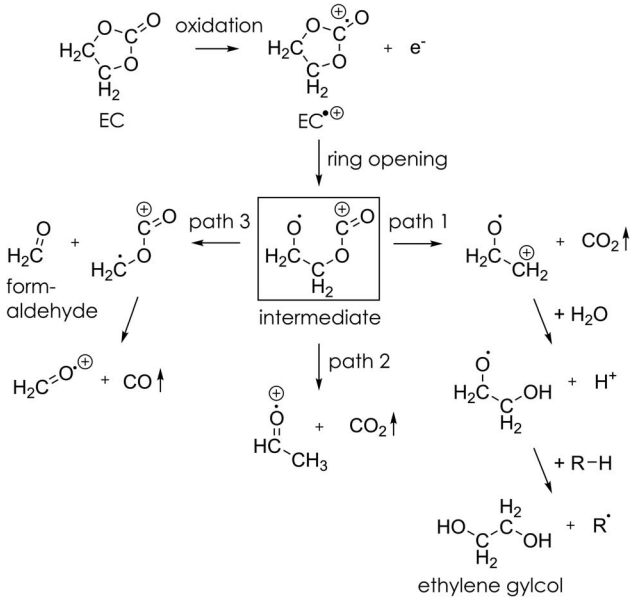

Scheme 1. Proposed mechanism for the anodic decomposition of ethylene carbonate to CO_2 and CO. Path 1 is favored in the presence of water, since its leaving group is stabilized by the nucleophilic attack of water eventually forming ethylene glycol.

Interestingly, Figure 5b and Table II show that in the presence of 4000 ppm H_2O much less ^{12}CO is evolved than $^{12}CO_2$, which might suggest that the presence of water favors one of the two depicted CO_2 formation pathways. Again, an unambiguous determination is only possible from our previous experiments with ^{13}C-labeled EC, where the CO_2/CO ratio from the anodic oxidation of EC with 4000 ppm H_2O at 25°C was found to be ≈12/1.[22] As depicted in Scheme 1, we believe that the presence of water, i.e. OH^- and H^+, in the oxidative environment of the polarized carbon electrode, favors reaction path 1, since it stabilizes the $^{\bullet}O\text{-}CH_2\text{-}CH_2^+$ leaving group by the formation of $^{\bullet}O\text{-}CH_2\text{-}CH_2\text{-}OH$ and H^+. Under the abstraction of an H• radical, e.g. from water or EC (generalized as R-H in Scheme 1), the obtained $^{\bullet}O\text{-}CH_2\text{-}CH_2\text{-}OH$ leaving group could be stabilized yielding ethylene glycol and R•. Further, the generated R• radicals might attack EC molecules leading to polymers, which could eventually passivate the electrode surface.[31] The reaction paths 2 and 3 are less likely to be favored by the presence of water, since their leaving groups do not offer any $-CH_2^+$ groups for the nucleophilic attack of water.

Carbon coating anodic oxidation mechanism.— Based on evidence from fuel cell literature[20,21] and from our recent work on the anodic oxidation of conductive carbon,[22] the expected oxidation reactions of carbon in the presence of water are summarized in Equations 1 and 2:

$$C + 2H_2O \rightarrow CO_2 \uparrow + 4H^+ + 4e^- \quad [1]$$

$$C + H_2O \rightarrow CO \uparrow + 2H^+ + 2e^- \quad [2]$$

In the H_2O-free electrolyte, 50 ppm of $^{13}CO_2$ and 20 ppm of ^{13}CO can be detected at the end of the LSV procedure (see Table II), with an onset of gas evolution at 4.75 V (see Figure 4b). As $^{13}CO_2$ and ^{13}CO isotopes can only originate from the ^{13}C-labeled carbon coating of LFP_^{13}C, it evidences that the anodic oxidation of the carbon coating even plays a role in electrolyte with very low water content (< 20 ppm H_2O). The $^{13}CO_2/^{13}CO$ molar ratio is ≈2.5/1, indicating a preference for the complete oxidation of carbon to CO_2 according to Reaction 1. Based on a mass balance, the amount of water in the electrolyte equates to $\approx 5.6 \cdot 10^{-7}$ mol (500 µl electrolyte or ≈0.5 g with 20 ppm H_2O), while the total amount of evolved $^{13}CO_2$ (50 ppm, see Table II) and ^{13}CO (20 ppm, see Table II) equate to $0.18 \cdot 10^{-7}$ mol and $0.07 \cdot 10^{-7}$ mol, respectively (based on 8.5 ml cell volume and 25°C). Therefore, despite its low concentration, there is a sufficient amount of water in the electrolyte for the anodic oxidation of the carbon coating to occur according to Reactions 1 and 2. On the other hand, in our previous study on the anodic oxidation of conductive carbon (Super C65) between 10 and 60°C in the same electrolyte (except that the EC was ^{13}C-labeled),[22] the amount of CO_2 (810 ppm $\equiv 2.9 \cdot 10^{-7}$ mol) and CO (310 ppm $\equiv 1.1 \cdot 10^{-7}$ mol) which was evolved at 60°C (see Table II in Reference 22) would require $6.9 \cdot 10^{-7}$ mol H_2O if formed via Reactions 1 and 2, which is much larger than the maximum amount of $\approx 2.7 \cdot 10^{-7}$ mol H_2O which was introduced through the electrolyte (240 µl electrolyte or ≈0.24 g with 20 ppm H_2O). This discrepancy suggests that either Reactions 1 and 2 are not the correct mechanisms for the anodic oxidation of carbon or that water must be produced "in situ" through the anodic oxidation of EC. The latter is rather likely, since it is generally believed that water is one of the anodic oxidation products of alkyl carbonates at potentials above 4.6 to 4.9 V.[35,36] That this is indeed the case will be shown in the next section.

In the presence of 4000 ppm H_2O, the onset of $^{13}CO_2/^{13}CO$ evolution moves negatively by ≈0.25 V to ≈4.5 V (see Figure 5b), again consistent with what one would expect based on Reactions 1 and 2. As in the case of electrolyte with < 20 ppm H_2O, the $^{13}CO_2/^{13}CO$ molar ratio is ≈2.5/1, as was also observed in our previous study with 4000 ppm H_2O for Super C65 carbon.[22] That the anodic oxidation of carbon might follow the same mechanism in electrolytes with < 20 ppm and with 4000 ppm H_2O is indicated by the very similar apparent activation energy which we observed in our previous study (≈65 kJ/mol vs. ≈54 kJ/mol for carbon in dry and 4000 ppm H_2O-containing electrolyte).[22] The observed similar apparent activation energies with and without water are thus another indication that in situ produced water might largely be responsible for the anodic oxidation of carbon, a hypothesis which will be examined in the following.

Formation of water by anodic decomposition of ethylene carbonate.— In the following, we will investigate the possible in situ formation of water as side-product during the anodic oxidation of ethylene carbonate. The difficulty in this endeavor is, that if water were produced at high potentials by the anodic oxidation of electrolyte, it might itself be oxidized ($H_2O \rightarrow 0.5O_2 + 2H^+ + 2e^-$),[22] forming highly reactive nascent oxygen which is likely to react before it can escape into the gas phase for mass spectrometric detection. For this reason, it is necessary to devise an in situ water detection probe, which has a sufficiently long life-time to escape into the gas phase for mass spectrometric detection. Our approach is thus based on the high reactivity between H_2O and PF_5, present in $LiPF_6$-based electrolytes,[37] and forming gaseous POF_3, which was shown to be

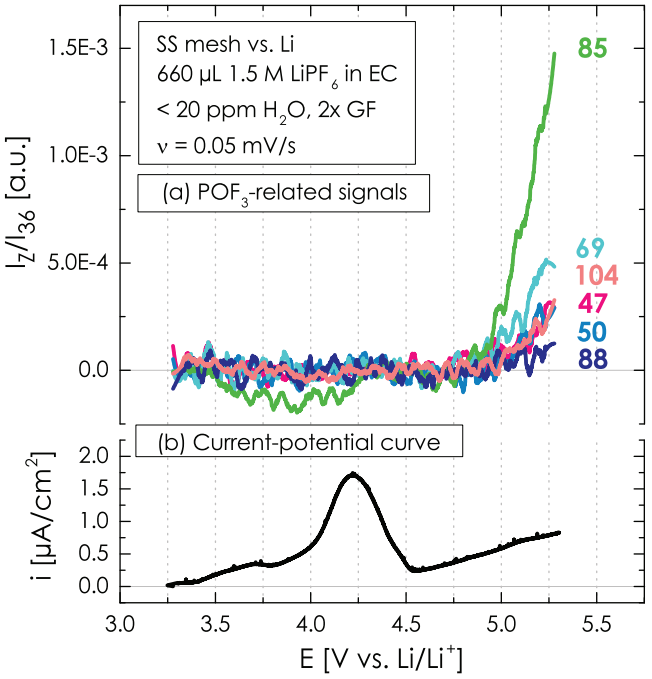

Figure 6. (a) Evolution of m/z = 104, 85, 69, 50, 47 and 88 as a function of potential for a SS mesh working-electrode vs. a metallic lithium counter-electrode with 500 µl of 1.5 M $LiPF_6$ in EC as electrolyte (< 20 ppm H_2O) in the working-electrode compartment and 160 µl in the counter-electrode compartment of the two-compartment cell, (b) corresponding current-potential curve for the linear potential sweep of the SS mesh working-electrode vs. the metallic lithium counter-electrode from 3.3 to 5.3 V vs. Li/Li^+ at 0.05 mV/s.

stable in EC-based electrolytes:[38]

$$LiPF_6 \rightarrow LiF + PF_5 \quad [3]$$

$$H_2O + PF_5 \rightarrow 2HF + POF_3 \uparrow \quad [4]$$

The occurrence of the above two reactions has also been confirmed in a recent study.[39] Based on these considerations, it should be possible to detect the formation of water in $LiPF_6$ based electrolytes by monitoring the evolution of POF_3, whose mass spectrometric fractionation pattern (m/z [%signal]) is: 104 [100%], 85 [80%], 69 [20%], 50 [< 10%], 47 [< 10%], 88 [< 5%].[40] This concept was tested using the sealed two-compartment cell with a 316L stainless steel (SS) mesh as working-electrode (diameter 21 mm, wire diameter 0.22 mm, openings 1.0 mm, Spörl KG, Germany), glass fiber separators, a metallic lithium counter-electrode, and EC with 1.5 M $LiPF_6$ as electrolyte (< 20 ppm H_2O as determined by Karl-Fischer titration).

Figure 6a shows the evolution of the POF_3-related m/z-channels upon a LSV scan from 3.3 to 5.3 V (see Figure 6b for current-potential curve). Starting from ≈4.75 V, the same potential as for the carbon coating oxidation without water (see Figure 4b), the traces of m/z = 104, 85, 69, 50, 47 and 88 start to increase. At 5.3 V, the signal of m/z = 85 reaches an I_{85}/I_{36} value of $1.5 \cdot 10^{-3}$, whereas the signal of m/z = 69 shows a three times lower I_{69}/I_{36} value of $0.5 \cdot 10^{-4}$, reasonably consistent with the above POF_3 fractionation pattern. Similarly consistent with the POF_3 fractionation pattern is the ≈2-fold lower I_{50}/I_{36} and I_{47}/I_{36} value and the ≈4-fold lower I_{88}/I_{36} value compared to the I_{69}/I_{36} value. On the other hand, the signal of m/z = 104 did not show a higher signal intensity than m/z = 85, as one would expect from the above POF_3 fractionation pattern. Since m/z = 104 corresponds to the singly ionized non-fragmented POF_3 (M = 104 g/mol), its lower than expected ion current is most probably related to the fact that our mass spectrometer is thermostated at ≈100°C, which would be expected to destabilize the singly ionized non-fragmented POF_3. Thus, we believe that the m/z-signals shown in Figure 6a are

Table III. Anodic oxidation rates of the carbon coating based on the sum of the $^{13}CO_2$ and ^{13}CO evolution rates at 4.8 and 5.0 V vs. Li/Li$^+$ and expressed in terms of: (i) measured rate in [ppm$_{(CO_2+CO)}$/h]; (ii) molar rate in [mol$_C$/s]; and, (iii) BET carbon surface area-normalized rate in [mol$_C$/(s · m^2_C]. The second to last column shows the projected weight loss of the carbon coating in [wt%$_C$/100 h]. All values were determined for dry electrolyte (< 20 ppm H_2O) and electrolyte containing 4000 ppm H_2O at 25°C. For comparison, the same quantities are given for the conductive carbon Super C65, calculated from data taken from Reference 22.

	Anodic oxidation rate based on sum of $^{13}CO_2 + {}^{13}CO$			
H_2O content	measured rate [ppm$_{(CO_2+CO)}$/h]	molar rate [mol$_C$/s]	projected mass loss [wt%$_C$/100 h]	BET-based rate [mol$_C$/(s · m^2_C)]
carbon coating at 4.8 V				
< 20 ppm H_2O	18	$0.17 \cdot 10^{-11}$	≈4	$0.14 \cdot 10^{-10}$
4000 ppm H_2O	67	$0.65 \cdot 10^{-11}$	≈15	$0.54 \cdot 10^{-10}$
carbon coating at 5.0 V				
< 20 ppm H_2O	36	$0.35 \cdot 10^{-11}$	≈8	$0.29 \cdot 10^{-10}$
4000 ppm H_2O	89	$0.86 \cdot 10^{-11}$	≈20	$0.72 \cdot 10^{-10}$
Super C65 at 5.0 V				
< 20 ppm H_2O	35	$0.34 \cdot 10^{-11}$	≈1	$0.28 \cdot 10^{-10}$
4000 ppm H_2O	265	$2.6 \cdot 10^{-11}$	≈6	$2.2 \cdot 10^{-10}$

indeed due to POF_3. The only other signals detected were m/z = 44 and 28, due to CO_2 and CO formation from electrolyte oxidation, and m/z = 19, which is most likely related to the formation of HF via Equation 4.[35] The measurement was reproduced with Celgard C480 separator instead of glass fiber separator and the same results were obtained (data not shown), so that any contribution of SiO_2 from the glass fiber separator can be excluded. In summary, POF_3 can serve as an in situ probe for the formation of water from the decomposition of alkyl carbonate electrolytes at high-voltage, whenever $LiPF_6$ is used as salt.

In a previous publication by our group,[35] we studied the anodic decomposition of trimethylboroxine (TMB), which is a known additive for improving the performance of $LiCoPO_4$. Our OEMS results suggested that TMB decomposes at potentials ≥ 4.5 V, producing large amounts of BF_3, POF_3, and CO_2 as well as H_2O and H_2. In the course of the TMB study, we already rationalized our observed formation of POF_3 by means of Equation 4, without, however, emphasizing that POF_3 is a useful marker for the onset and extent of water formation.

Projected weight loss of carbon coating in high-voltage cathodes.— In the light of the above results for the anodic oxidation of the carbon coating on LFP particles, the stability of carbon coated high-voltage materials like $LiCoPO_4$ operating between 4.8 and 5.0 V vs. Li/Li$^+$ can be dramatic. Since the anodic oxidation product of carbon will be either CO_2 or CO, the sum of the $^{13}CO_2$ and ^{13}CO evolution rates at any given potential will be a quantitative measure of the carbon oxidation rate under these conditions. The $^{13}CO_2$ and ^{13}CO evolution rates at a given potential can be determined from the slope of the gas concentration vs. potential in Figures 4b and 5b, and their values in terms of the total $^{13}CO_2 + {}^{13}CO$ evolution rates in units of [ppm$_{CO_2+CO}$/h] are shown in Table III (2nd column) for 4.8 and 5.0 V, based on a linear regression fit at 4.8 V ± 25 mV and 5.0 V ± 25 mV and considering the scan rate of 0.05 mV/s. The so obtained anodic oxidation rate of the carbon coating at each potential increases by a factor of ≈3 when increasing the water content from < 20 ppm to 4000 ppm, consistent with Reactions 1 and 2 and similar to what would be expected on the basis of Table II.

In order to project the carbon coating loss over time, we first convert the measured anodic oxidation rate into a molar carbon oxidation rate in units of [mol$_C$/s] (see 3rd column in Table III), using the volume of the employed cell (viz., 8.5 ml, corresponding to $3.5 \cdot 10^{-4}$ mol$_{gas}$ at 25°C and 1 bar). Multiplying the molar carbon oxidation rate by the molecular weight of ^{13}C carbon (13 g/mol) and normalizing the obtained mass-based carbon oxidation rate by the total mass of carbon coating in the cell (0.2 mg, based on 15 mg$_{LFP}$/cm$^2 \cdot 1.33$ cm^2 = 20 mg$_{LFP}$ with a 1 wt% carbon coating according to Table I), one can project the mass loss of the carbon coating over a 100 h hold time at either 4.8 or 5.0 V (in units of [wt%$_C$/100 h], see 4th column of Table III). Based on these projections, the weight loss of a carbon coating on a high-voltage cathode material operating at 4.8 V in H_2O-free electrolyte (< 20 ppm H_2O) would amount to ≈4 wt% over 100 h or ≈20 wt% over 500 h. This should result in a substantial loss of electrical conductivity between the primary particles of the active material and the conductive carbon additives, and is likely to negatively affect the long-term rate capability, i.e., the long-term performance particularly at high C-rates. At the higher voltage of 5.0 V, the projected rate of weight loss of the carbon coating doubles, amounting to ≈8 wt% over 100 h (see 4th column of Table III) or ≈40 wt% over 500 h. Therefore, our analysis suggests that carbon coatings on high-voltage cathode materials are probably not sufficiently stable against anodic oxidation even in nominally dry electrolytes.

The above projected weight loss of the carbon coating is of course specific to the actually used cathode material (i.e., to LFP_^{13}C in our study). However, considering that the oxidation rate for the same type of carbon coating should be proportional to the exposed surface area, the weight loss is expected to be proportional to the specific surface area (i.e., the BET area) of the active material (6 m^2/g for LFP_^{13}C, see Table I) onto which the coating is applied. In addition, the projected weight loss will be inversely proportional to the carbon content (1 wt% for LFP_^{13}C, see Table I). Thus, the projected carbon coating weight loss rate obtained in this study (r_{exp} [wt%/100 h], second to last column in Table III) can be used to estimate the carbon coating weight loss rate ($r_{C\text{-}coating}$) for carbon coatings on any high-voltage cathode material:

$$r_{C\text{-}coating}\,[\text{wt\%}/100\,\text{h}] = r_{exp}\,[\text{wt\%}/100\,\text{h}] \cdot \left(x\left[\text{m}^2/\text{g}\right] / 6\left[\text{m}^2/\text{g}\right]\right) \cdot (1\,[\text{wt\%}] / y\,[\text{wt\%}]) \quad [5]$$

where x refers to the specific surface area of the high-voltage cathode material and y refers to the wt% of the applied carbon coating. For example, if one were to consider an active material with a BET area of 0.8 m^2/g and a carbon coating at a level of 2.5 wt% carbon, the projected weight loss rate at 4.8 V in electrolyte with < 20 ppm H_2O would be ≈0.2 wt% over 100 h, i.e., 20-fold lower than the 4 wt% listed in Table III for our LFP_^{13}C. This suggests that a carbon coating on a high-voltage cathode material might have acceptable long-term stability, as long as its specific surface area is very low. This, however, is unlikely possible for high-voltage phospho-olivines like LCP, which typically require rather high specific surface areas.

A last open question is to what extent the anodic carbon oxidation rates depends on the type of carbon. Based on the fuel cell literature, one would expect that the carbon oxidation rate depends mostly on the exposed carbon surface area and very little on the specific type of carbon.[41] In this case, the BET surface area-normalized carbon oxidation rate in units of [mol$_C$/(s · m^2_C)] would be the intrinsic rate expression, which is obtained by dividing the molar rate (in units of

[mol_C/s], see Table III) by the exposed carbon surface area. In this study, the carbon surface area in the cell is 0.12 m^2 (viz., 0.2 mg carbon coating on 20 mg LFP at a specific surface area of 6 m^2/g; the tacit assumption of a homogeneous carbon coating is supported by our Raman data), from which the BET-normalized anodic oxidation rate can be calculated (see last column in Table III). Its value of $0.29 \cdot 10^{-10}$ [$mol_C/(s \cdot m^2_C)$] at 5.0 V in electrolyte with < 20 ppm H_2O is in excellent agreement with that obtained under identical conditions for the commonly used conductive carbon, Super C65 (68 m^2_C/g) which we had determined in our recent work[22] (see last column in Table III). The fact that our carbon coating and Super C65 seem to have a similar stability against anodic oxidation, is further supported by Raman spectroscopy, where they show a similar degree of graphitization (data not shown). The cause for the ≈3-fold difference in the presence of 4000 ppm H_2O is unfortunately not clear at this point.

Conclusions

In this work, we synthesized $LiFePO_4$ (LFP) with an isotopically labeled ^{13}C carbon coating as a model compound to quantify the anodic oxidation of a carbon coating at high-voltage by measuring the evolution of $^{13}CO_2$ and ^{13}CO via On-line Electrochemical Mass Spectrometry (OEMS). It was shown that the addition of 4000 ppm H_2O to a model electrolyte comprised of ethylene carbonate and 1.5 M $LiClO_4$, significantly enhances the carbon coating oxidation. At a potential of 4.8 V, corresponding to the operating voltage of high-voltage cathode materials like $LiCoPO_4$ (LCP), the anodic oxidation of a carbon coating in dry electrolyte would lead to a loss of ≈4 wt% over 100 h, while 4000 ppm H_2O in the electrolyte would increase the carbon coating loss to ≈15 wt% over 100 h.

Furthermore, we could show that the anodic decomposition of ethylene carbonate (EC) at potential $\geq$ 4.75 V leads to the generation of water, which we evidenced by the formation of gaseous POF_3, formed by the reaction of $LiPF_6$ with in situ produced H_2O. Our data suggest that a carbon coating on high-voltage cathode materials will not have sufficient long-term stability in EC-containing electrolytes, since a significant fraction of the carbon coating will be oxidized, especially at potentials $\geq$ 4.75 V where carbon oxidation is triggered by in situ produced water. Generally, the formation of water at high potentials needs to be considered for understanding the capacity fade of high-voltage cathode materials. Both, the HF formation in F-containing electrolyte and the loss of electrical conductivity due to carbon coating oxidation are detrimental for long-term cycling stability.

Acknowledgment

The authors thank BMW for financial support and Clariant for providing the commercial $LiFePO_4$ material. We further acknowledge Katia Rodewald (WACKER-Chair of Molecular Chemistry at TUM) for the SEM pictures, Ulrike Ammari (analytical lab of TUM at the Chair of Inorganic Chemistry) for the CHNS analyses, and Sebastian Schwaminger (Bioseparation Engineering Group at TUM) for the Raman spectra. Brett Lucht (University of Rhode Island) and Sophie Solchenbach (Chair of Technical Electrochemistry at TUM) are gratefully acknowledged for helpful discussions.

References

1. J.-M. Tarascon and M. Armand, *Nature*, **414**, 359 (2001).
2. L. Lu, X. Han, J. Li, J. Hua, and M. Ouyang, *Journal of Power Sources*, **226**, 272 (2013).
3. M. S. Whittingham, *Chem. Rev.*, **104**, 4271 (2004).
4. D. Liu, W. Zhu, J. Trottier, C. Gagnon, F. Barray, A. Guerfi, A. Mauger, H. Groult, C. M. Julien, J. B. Goodenough, and K. Zaghib, *RSC Adv.*, **4**, 154 (2014).
5. J. Xu, S. Dou, H. Liu, and L. Dai, *Nano Energy*, **2**, 439 (2013).
6. S. Brutti and S. Panero, *Nanotechnology for Sustainable Energy (ACS Symposium Series)*, chapter **4**, 68 (2013).
7. H. Li and H. Zhou, *Chem. Comm.*, **48**, 1201 (2012).
8. R. Dominko, M. Bele, M. Gaberscek, M. Remskar, D. Hanzel, S. Pejovnik, and J. Jamnik, *J. Electrochem. Soc.*, **152**, A607 (2005).
9. K. Zaghib, A. Mauger, H. Groult, J. B. Goodenough, and C. M. Julien, *Materials*, **6**, 1028 (2013).
10. Z. Chen and J. Dahn, *J. Electrochem. Soc.*, **149**, A1184 (2002).
11. Y. Lin, M. X. Gao, D. Zhu, Y. F. Liu, and H. G. Pan, *Journal of Power Sources*, **184**, 444 (2008).
12. H. C. Shin, W. I. Cho, and H. Jang, *Electrochimica Acta*, **52**, 1472 (2006).
13. X. Lou and Y. Zhang, *J. Mater. Chem.*, **21**, 4156 (2011).
14. Z. Y. Chen, H. L. Zhu, S. Ji, R. Fakir, and V. Linkov, *Solid State Ionics*, **179**, 1810 (2008).
15. J. Wolfenstine, J. Read, and J. L. Allen, *Journal of Power Sources*, **163**, 1070 (2007).
16. N. N. Bramnik, K. Nikolowski, D. M. Trots, and H. Ehrenberg, *Electrochem. Solid State Lett.*, **11**, A89 (2008).
17. S. Theil, M. Fleischhammer, P. Axmann, and M. Wohlfahrt-Mehrens, *Journal of Power Sources*, **222**, 72 (2013).
18. C. Stinner, P. Axmann, M. Mehrens, W. Weirather, and M. Fleischhammer, Pat. DE102011106326B3 (2013).
19. N. Tsiouvaras, S. Meini, I. Buchberger, and H. A. Gasteiger, *J. Electrochem. Soc.*, **160**, A471 (2013).
20. K. Kinoshita, *Carbon – Electrochemical and Physicochemical Properties*, chapter 6.3, JohnWiley&Sons, Berkley California USA (1987).
21. S. Zhang, X. Z. Yuan, J. N. Cheng Hin, H. Wang, K. A. Friedrich, and M. Schulze, *Journal of Power Sources*, **194**, 588 (2009).
22. M. Metzger, C. Marino, J. Sicklinger, D. Haering, and H. A. Gasteiger, *J. Electrochem. Soc.*, **162**, A1123 (2015).
23. K. Xu, *Chem. Rev.*, **104**, 4303 (2004).
24. G. Liang, L. Wang, X. Ou, X. Zhao, and S. Xu, *Journal of Power Sources*, **184**, 538 (2008).
25. A. S. Andersson, B. Kalska, L. Haggstrom, and J. O. Thomas, *Solid State Ionics*, **130**, 41 (2000).
26. Y. Bai, Y. Yin, J. Yang, C. Qing, and W. Zhang, *Journal of Raman Spectroscopy*, **42**, 831 (2011).
27. B. Ellis, W. H. Kan, W. R. M. Makahnouk, and L. F. Nazar, *J. Mater. Chem.*, **17**, 3248 (2007).
28. R. Kostecki, B. Schnyder, D. Alliata, X. Song, K. Kinoshita, and R. Kötz, *Thin Solid Films*, **396**, 36 (2001).
29. C. M. Julien, K. Zaghib, A. Mauger, M. Massot, A. Ait-Salah, M. Selmane, and F. Gendron, *J. Appl. Phys.*, **100**, 63511 (2006).
30. A. Ait Salah, A. Mauger, K. Zaghib, J. B. Goodenough, N. Ravet, M. Gauthier, F. Gendron, and C. M. Julien, *J. Electrochem. Soc.*, **153**, A1692 (2006).
31. M. Moshkovich, M. Cojocaru, H. E. Gottlieb, and D. Aurbach, *J. Electroanal. Chem.*, **497**, 84 (2001).
32. L. Xing, W. Li, C. Wang, F. Gu, M. Xu, C. Tan, and J. Yi, *J. Phys. Chem. B*, **113**, 16596 (2009).
33. Y. L. Yang, S. G. Ramaswamy, and W. B. Jakoby, *J. Biol. Chem.*, **273**, 7814 (1998).
34. X. Zhang, J. K. Pugh, and P. N. Ross, *J. Electrochem. Soc.*, **148**, E183 (2001).
35. A. Freiberg, M. Metzger, D. Haering, S. Bretzke, T. Nilges, C. Stinner, C. Marino, and H. A. Gasteiger, *J. Electrochem. Soc.*, **161**, A2255 (2014).
36. E. Markevich, R. Sharabi, H. Gottlieb, V. Borgel, K. Fridman, G. Salitra, D. Aurbach, G. Semrau, M. A. Schmidt, N. Shall, and C. Bruenig, *Electrochem. Comm.*, **15**, 22 (2012).
37. S. E. Sloop, J. K. Pugh, S. Wang, J. B. Kerr, and K. Kinoshita, *Electrochem. Solid State Lett.*, **4**, A42 (2001).
38. H. Yang, G. V. Zhuang, and P. N. Ross Jr., *Journal of Power Sources*, **161**, 573 (2006).
39. S. F. Lux, I. T. Lucas, E. Pollak, S. Passerini, M. Winter, and R. Kostecki, *Electrochem. Commun.*, **14**, 47 (2012).
40. NIST Mass Spec Data Center, S. E. Stein, director, "Mass Spectra" in NIST Chemistry WebBook, NIST Standard Reference Database Number 69, Eds. P. J. Linstrom and W. G. Mallard, National Institute of Standards and Technology, Gaithersburg MD, 20899, http://webbook.nist.gov, (retrieved 2014).
41. P. T. Yu, W. Gu, J. Zhang, R. Makharia, F. T. Wagner, and H. A. Gasteiger, Carbon-Support Requirements for Highly Durable Fuel Cell Operation, in *Polymer Electrolyte Fuel Cell Durability* (eds. F. N. Buechi, M. Inaba, and T. J. Schmidt), 29, Springer, New York (2009).